Ca²⁺-Dependent Interaction of S100A1 with F₁-ATPase Leads to an Increased ATP Content in Cardiomyocytes[▽]

Melanie Boerries,[1,2]† Patrick Most,[3,4]† Jonathan R. Gledhill,[5] John E. Walker,[5] Hugo A. Katus,[4] Walter J. Koch,[3] Ueli Aebi,[1] and Cora-Ann Schoenenberger[1]*

Maurice E. Mueller Institute, Biozentrum, University of Basel, 4056 Basel, Switzerland[1]; Institute for Pharmacology and Toxicology, University of Freiburg, 79104 Freiburg, Germany[2]; Center for Translational Medicine, Department of Medicine, Thomas Jefferson University, Philadelphia, Pennsylvania 19107[3]; Department of Internal Medicine III, Division of Cardiology, University of Heidelberg, 69115 Heidelberg, Germany[4]; and Medical Research Council Dunn Human Nutrition Unit, Wellcome Trust/MRC Building, Hills Road, Cambridge CB2 2XY, United Kingdom[5]

S100A1, a Ca²⁺-sensing protein of the EF-hand family that is expressed predominantly in cardiac muscle, plays a pivotal role in cardiac contractility in vitro and in vivo. It has recently been demonstrated that by restoring Ca²⁺ homeostasis, S100A1 was able to rescue contractile dysfunction in failing rat hearts. Myocardial contractility is regulated not only by Ca²⁺ homeostasis but also by energy metabolism, in particular the production of ATP. Here, we report a novel interaction of S100A1 with mitochondrial F₁-ATPase, which affects F₁-ATPase activity and cellular ATP production. In particular, cardiomyocytes that overexpress S100A1 exhibited a higher ATP content than control cells, whereas knockdown of S100A1 expression decreased ATP levels. In pull-down experiments, we identified the α- and β-chain of F₁-ATPase to interact with S100A1 in a Ca²⁺-dependent manner. The interaction was confirmed by colocalization studies of S100A1 and F₁-ATPase and the analysis of the S100A1–F₁-ATPase complex by gel filtration chromatography. The functional impact of this association is highlighted by an S100A1-mediated increase of F₁-ATPase activity. Consistently, ATP synthase activity is reduced in cardiomyocytes from S100A1 knockout mice. Our data indicate that S100A1 might play a key role in cardiac energy metabolism.

S100 proteins are a family of soluble, EF-hand Ca²⁺-binding proteins which exhibit a remarkable cell- and tissue-specific expression pattern. They are involved in numerous intracellular activities, such as cell proliferation and differentiation, or the dynamics of cytoskeletal constituents (reviewed in references 4, 9, and 30). The most abundant S100 protein in the heart is S100A1 (12; reviewed in reference 4). It has been recognized recently as a positive inotropic intracellular regulator of cardiac as well as skeletal muscle Ca²⁺ homeostasis and contractility (15, 16, 18, 19, 20). Accordingly, S100A1-deficient mice exhibited an impaired cardiac contractility response to hemodynamic stress (5). Notably, the absence of S100A1 significantly accelerates the development of contractile dysfunction after myocardial infarction, with a rapid onset of cardiac remodeling and a transition to heart failure combined with excessive mortality (21). Normal contractile function and Ca²⁺ homeostasis, on the other hand, could be restored in failing myocardium in postinfarcted rat hearts by S100A1 gene delivery (19).

In addition to Ca²⁺ homeostasis, myocardial workload depends on cardiac metabolism. As the energy demand changes, the flux through the mitochondrial ATP synthase (F₁Fₒ-ATPase), which is responsible for the bulk of ATP synthesis in the myocardium, must change so that ATP synthesis matches

ATP consumption (reviewed in references 6 and 10). To sustain cardiac function in all possible situations, there has to be a strict correlation between energy production, energy transfer, and energy utilization (reviewed in reference 29). In this regard, Ca²⁺ has emerged as a major factor for adapting mitochondrial ATP production to the constantly varying energy demand of the cell. Consistently, several studies provided evidence that F₁Fₒ-ATPase-dependent ATP synthesis correlates with Ca²⁺ levels in heart cells (reviewed in reference 1). Furthermore, metabolic pathway abnormalities that result in an imbalance of several metabolic reactions, for example, a decreased phosphocreatine/ATP ratio, indicative of an increase in ADP, an alteration of oxidative phosphorylation, and a decreased ATP/ADP ratio, lead to abnormal contraction and relaxation and eventually result in the failing of the heart. Thus, it is conceivable that energy starvation may contribute to heart failure (reviewed in reference 11).

Because S100A1 is able to restore a reduced phosphocreatine/ATP ratio and Ca²⁺ homeostasis in failing cardiomyocytes (19), we examined whether S100A1 has an influence on cardiac energy homeostasis in neonatal rat ventricular cardiomyocytes (NVCMs). Here, we demonstrate a Ca²⁺-dependent interaction of S100A1 with the α- and β-chain of the F₁-ATPase in NVCMs and isolated mitochondria. Moreover, this interaction is consolidated by colocalization in immunofluorescence and immunoelectron microscopy studies and the isolation of an S100A1–F₁-ATPase complex by gel filtration chromatography. Furthermore, the physiological significance of S100A1 in energy metabolism is validated through the effects of S100A1 overexpression and knock-

---

* Corresponding author. Mailing address: Maurice E. Mueller Institute for Structural Biology, Biozentrum, University of Basel, 4056 Basel, Switzerland. Phone: 0041-612672096. Fax: 0041-612672109. E-mail: cora-ann.schoenenberger@unibas.ch.
† These authors contributed equally to this study.

down on ATP production in NVCMs and its influence on F$_1$-ATPase activity.

Based on the data presented, a new role for S100A1 in cardiac energy metabolism emerges.

MATERIALS AND METHODS

Reagents. ATP (disodium salt), phosphoenolpyruvate, NADH, pyruvate kinase, lactate dehydrogenase, and isoproterenol were purchased from Sigma.

Generation of an S100A1 adenovirus. The generation of an S100A1 adenovirus (AdS100A1) by the pAdTrack-CMV/pAdEasy-1 system has been described elsewhere (15). To facilitate the identification of infected cells, AdS100A1 carried the green fluorescent protein (GFP) reporter gene in addition to the human S100A1 cDNA (GenBank accession number X58079). Each transgene was independently expressed under the control of a cytomegalovirus promoter sequence. To rule out the possibility that the infection procedure itself had an effect on the amount of S100A1 in the cell, cells were infected with the corresponding adenovirus carrying GFP cDNA alone as a control (Adcontrol).

Isolation and primary culture of NVCMs and adult mice. Ventricular cardiomyocytes from 1- to 2-day-old neonatal hearts (NVCMs) were isolated as described in detail elsewhere (17). NVCMs were cultured in Dulbecco's modified Eagle's medium supplemented with penicillin-streptomycin (100 units/ml), L-glutamine (2 mM), and 1% fetal calf serum (FCS Gold; PAA Laboratories GmbH) at 37°C in a 95% air-5% CO$_2$ humidified atmosphere for 2 to 3 days. Adenoviral infection of NVCMs was carried out in serum-free M199 medium with a multiplicity of infection of 8 PFU per cell. After 4 h of incubation at 37°C, M199 medium was changed to Dulbecco's modified Eagle's medium supplemented with penicillin-streptomycin (100 units/ml), L-glutamine (2 mM), and 1% fetal calf serum. The efficiency of adenoviral gene transfer was monitored 24 h later by GFP fluorescence. Accordingly, approximately 95% of NVCMs were infected.

S100A1-deficient (SKO) mice have previously been described (5). Adult ventricular cardiomyocytes from C57BL/6 wild-type (WT) and SKO mice (2 to 3 months of age) were enzymatically isolated using a pressure- and temperature-controlled retrograde coronary perfusion protocol as reported elsewhere (24). Subsequently, WT and SKO cardiomyocytes were pelleted and sonicated in ice-cold EGTA-buffered sonication solution (20 mM HEPES, 1.0 MgCl$_2$, 2.0 mM EGTA, pH 7.2) with a free [Ca^{2+}] of 0.2 mM. Samples were kept on ice until measurements. Free [Ca^{2+}] was calculated by applying the program REACT.

S100A1 RNA interference. Custom-designed synthetic S100A1 small interfering RNA (siRNA) and scrambled siRNA as a negative control were purchased from Eurogentec. S100A1 siRNA is target-specific 20- to 25-nucleotide siRNA to knock down the gene expression of S100A1 in NVCMs (sense, 5′-UGG AGA CCC UCA UCA AUG UdTdT-3′; antisense, 5′-ACA UUG AUG AGG GUC UCC AdTdT-3′). NVCMs were transfected with S100A1 and control siRNA oligonucleotides (100 nM) by using Effectene transfection reagent according to the manufacturer's instructions (QIAGEN). After incubation at 37°C for 24 h, cells were lysed and subjected to Western blotting.

Indirect immunofluorescence. Immunofluoresence labeling of NVCMs was carried out as previously described (17). Freshly isolated NVCMs were cultured for 2 days on glass coverslips and incubated with the fluorescent dye MitoTracker Red (1 μM; Molecular Probes) for 30 min. Cells were fixed, permeabilized, and labeled with a monoclonal anti-S100A1 antibody (diluted 1:200; Sigma) and a polyclonal F$_1$-ATPase antibody (diluted 1:400). The latter was a kind gift from Pfanner (Institute for Biochemistry and Molecular Biology, Freiburg, Germany). The secondary antibodies used were Alexa Fluor 488-conjugated anti-mouse immunoglobulin (diluted 1:800; Alexis) and Cy5-conjugated anti-rabbit immunoglobulin (diluted 1:400; Jackson ImmunoResearch Lab). Confocal images were obtained using a 100× oil objective lens on a Leica TCS SP laser scanning confocal microscope. Digitized confocal images were processed by Leica software and Adobe Photoshop.

Immunoelectron microscopy. Isolated mitochondria and pieces of heart tissue from 3-day-old neonatal rats were fixed as previously described (25). Ultrathin sections were cut and mounted on carbon-Parlodion-coated copper grids. Specimens were blocked with 2% bovine serum albumin (BSA) in phosphate-buffered saline (PBS) two times for 5 min prior to incubation with S100A1 antibody (diluted 1:100; Sigma) for 2 h at room temperature (RT). Grids were washed in PBS, blocked in 2% BSA in PBS two times for 5 min, and then incubated with 10 nm gold-conjugated goat anti-mouse secondary antibody (BBInternational) for 1 h at RT.

For double immunolabeling, sections were sequentially incubated with the primary antibodies and the corresponding gold-conjugated secondary antibody

(10 nm and 5 nm, respectively) for 2 h at RT. After being washed in PBS and water, grids were stained with a mixture of 6% uranyl acetate for 1 h, rinsed with water, and then poststained for 2 min with lead citrate. Electron micrographs were recorded on a Hitachi 7000 at 80 kV.

Isolation of mitochondria. Mitochondria were isolated from the hearts of adult male rats by differential centrifugation steps as described previously (3). Briefly, minced heart tissue was homogenized with approximately 10 ml/g tissue homogenization buffer (0.1 M KCl, 0.05 M MOPS [morpholinepropanesulfonic acid], 5 mM MgSO$_4$, 1 mM EDTA, 1 mM ATP, 0.2% BSA, pH 7.4), using a Teflon glass homogenizer with a loose-fitting piston. The homogenate was centrifuged at 300 × g at 4°C for 10 min. The supernatant was poured through a double-layered cheese cloth and centrifuged again at 5,000 × g at 4°C for 10 min. Pelleted mitochondria were resuspended in 1 ml homogenization buffer and centrifuged again at 5,000 × g at 4°C for 10 min. The pellet was resuspended in 0.15 ml KME buffer (0.1 M KCl, 0.05 M MOPS, 0.5 mM EGTA, pH 7.4). The protein concentration in the mitochondrial suspension was determined by the Bradford method (Sigma), using bovine albumin fraction V as a standard.

Purification of F$_1$-ATPase/S100A1–F$_1$-ATPase complex and F$_1$-ATPase activity. Purification of the bovine F$_1$-ATPase was carried out as previously described (22). The S100A1–F$_1$-ATPase complex was prepared as follows. Purified F$_1$-ATPase (15 mg), stored as an ammonium sulfate precipitate, was collected by centrifugation (16,000 × g), redissolved in complex buffer (20 mM Tris, pH 7.4, 100 mM NaCl, 1 mM MgCl$_2$, 2 mM CaCl$_2$), and desalted on a Micro Bio-Spin column (Amersham Pharmacia Biotech). The enzyme was then mixed with a 12.5-fold molar excess of S100A1 over F$_1$-ATPase and incubated for 30 min at 37°C. MgATP (1 mM) was added at 1 and 15 min to yield a final concentration of 2 mM. ATPase activity was measured at 37°C with an ATP-regenerating system as reported by following the oxidation of NADH to NAD$^+$ at 340 nm in a Hewlett-Packard spectrophotometer (2). The assay was carried out in 1 ml assay buffer (50 mM Tris, pH 7.4, 50 mM KCl, 2 mM MgCl$_2$) containing 2 mM ATP, 2 mM phosphoenolpyruvate, 0.4 mM NADH, 12.5 U pyruvate kinase, and 12.5 U lactate dehydrogenase. The reaction was started by adding 10 μl of F$_1$-ATPase or the S100A1–F$_1$-ATPase complex in the presence of 2 mM or 0.2 mM CaCl$_2$. The decline of NADH absorbance at 340 nm allows for monitoring of the rate of ATP hydrolysis (optical density/min).

Determination of mitochondrial ATP synthase activity. The enzymatic activity of the mitochondrial ATP synthase complex was measured using a spectrophotometric assay as described elsewhere with minor modifactions (7). Briefly, aliquots of cardiomyocyte homogenates from adult WT and SKO mice were added to EGTA-buffered activity solution (in mM: 60 sucrose, 50 triethanolamine-HCl, 50 KCl, 4 MgCl$_2$, 2 ATP, 1.5 phosphoenolpyruvate, 2 EGTA, 1 KCN, 0.001 thapsigargin, pH 7.4, with KOH) supplemented with 200 μM NADH, 5 U pyruvate kinase, and 5 U lactate dehydrogenase. Thapsigargin was used to block the activity of the Ca^{2+}-sensitive sarcoplasmic reticulum Ca^{2+} ATPase. Free [Ca^{2+}] was adjusted to either 0.2 μM or 0.2 mM, determined by the program REACT. The conversion of NADH to NAD$^+$ was followed spectrophotometrically at 340 nm at 37°C for 3 min. Recombinant human S100A1 protein was added 10 min prior to measurement as indicated. Oligomycin (10 μg/ml) was used to block the mitochondrial ATP synthase. Mitochondrial ATP synthase activity was calculated as the difference between total and oligomycin-insensitive conversion of NADH to NAD$^+$.

Gel filtration chromatography. Upon its preparation as described above, the S100A1–F$_1$-ATPase complex was chromatographed at RT at a flow rate of 0.3 ml/min on a HiLoad Superdex 200 column that was preequilibrated in complex buffer. The absorbance of the eluant was monitored at 280 nm. Individual fractions (0.3 ml) were analyzed by sodium dodecyl sulfate-polyacrylamide gel electrophoresis (SDS-PAGE).

Measurement of ATP production. The ATP content of NVCMs was determined by the luciferin-luciferase system according to the manufacturer's protocol (ATP bioluminescence assay kit HS II; Roche).

Recombinant proteins. A human S100A1 cDNA (accession number X58079) was subcloned into the expression vector pGEX-6P1 containing glutathione S-transferase (GST) cDNA. S100A1 was produced as a fusion protein with a 26-kDa GST at the NH$_2$ terminus (GST-S100A1) by an isopropyl-β-D-thiogalactopyranoside (IPTG)-driven expression system in *Escherichia coli*. The fusion protein was purified using glutathione-Sepharose 4B (Amersham Pharmacia Biotech) and dialyzed against PBS.

The GST fusion constructs of palpha3 and pbeta1 were generated by PCR overlap extension using cDNAs of the α- and β-chain of mitochondrial bovine heart F$_1$-ATPase (palpha3 and pbeta1). The two external primers for the palpha3 construct used were as follows: 5′ EcoRI primer, 5′-GAATTCCAGAAA CCGGCACT, and 3′ XhoI primer, 5′-CTCGAGAGCTTC AAATCCAGC. The PCR product was digested with EcoRI and XhoI and inserted into the pGEX-

6P1 vector at the corresponding restriction sites. For the GST-pbeta1 expression construct, the two external primers were as follows: 5′ SalI primer, 5′-CGGTC GACTCATGGCCGCTCAAGCATCTCC, and 3′ NotI primer, 3′-CCCGCCG GCCGCTCATGAGTGCTCTTCAGCCAAC. The PCR product was digested with SalI and NotI and inserted into the pGEX-6P1 vector at the respective sites. GST fusion proteins of the α-chain and β-chain of F_1-ATPase were expressed and purified as described for GST-S100A1.

A recombinant human S100A1 cDNA (accession number X58079) was also subcloned into the expression vector pHis-TRX-1 containing a thrombin cleavage side. S100A1 was produced as a fusion protein with a histidine tag at the NH_2 terminus by an IPTG-driven expression system in *E. coli*. The fusion protein was purified using a HiTrap chelating HP column (Amersham Pharmacia Biotech) according to the manufacturer's protocol. Subsequently, the histidine tag was removed by thrombin cleavage and purified S100A1 was dialyzed against 25 mM Tris, pH 7.45.

GST pull-down assays. GST fusion proteins (0.02 mg/ml GST-S100A1, GST– α–F_1-ATPase, and GST–β–F_1-ATPase) or GST alone was bound to glutathione *S*-Sepharose slurries in an incubation buffer (IB2; 100 mM NaCl, 20 mM Tris, pH 7.4, 0.05% Triton X-100, containing 2 mM $CaCl_2$, 0.2 mM $CaCl_2$, or 2 mM EGTA) for 1.5 h at 4°C. Isolated neonatal rat cardiomyocytes (5×10^6 cells) and 1 mg/ml isolated heart mitochondria were homogenized in a homogenization buffer (100 mM NaCl, 20 mM Tris, pH 7.4, 1 mM $MgCl_2$, 1 mM phenylmethyl-sulfonyl fluoride, 1 μl DNase, 0.2% Triton X-100, supplemented with a Complete mini EDTA-free protease inhibitor tablet; Roche) containing 2 mM $CaCl_2$, 0.2 mM $CaCl_2$, or 2 mM EGTA. Homogenates of neonatal cardiomyocytes, isolated mitochondria, and recombinant S100A1 (1 μM) were incubated with GST-S100A1, GST–α–F_1-ATPase, GST–β–F_1-ATPase, or GST slurries for 2.5 h at 4°C. Incubation of purified F_1-ATPase with GST-S100A1 or GST slurries was carried out at RT for 1 h. Mixtures were washed six times with IB2, applied to spin columns, and centrifuged at $400 \times g$ for 1 min. The columns were spin washed twice with IB2. Unbound protein was removed by spin wash steps for 3 min at $2,300 \times g$. Bound proteins were eluted with SDS-PAGE sample buffer (5% SDS) and analyzed by SDS-PAGE and mass spectrometry.

Mass spectrometry analysis. For mass spectrometry, gel slices were excised from silver-stained SDS-PAGE gels and digested with 0.25 μg trypsin (Promega) in 50 mM ammonium bicarbonate (pH 8.0) at 37°C for 16 h. The resulting peptides were analyzed by capillary liquid chromatography/tandem mass spectrometry (MS/MS), using a Magic C_{18} 100-μm by 10-cm high-performance liquid chromatography column (Spectronex) connected to a Finnigan TSQ7000 tandem mass spectrometer (ThermoFinnigan). A linear gradient from 2 to 75% buffer B (0.1% acetic acid and 80% [vol/vol] acetonitrile in water) in buffer A (0.1% acetic acid in water) was generated with a Rheos 2000 high-pressure liquid chromatography system (Flux) at 100 μl/min. A precolumn flow splitter reduced the flow to approximately 500 nl/min. The eluting peptides were ionized by electrospray ionization and detected, and the peptides were automatically selected and fragmented by collision-induced dissociation (MS/MS). Individual MS/MS spectra were searched in the data bank using Mascot software (http://www.matrixscience.com).

Western blotting. To reveal the presence of S100A1 in the SDS-PAGE-separated protein mixtures of pull-down experiments, standard Western blotting using a specific polyclonal anti-S100A1 antibody (SA 5632, diluted 1:10,000; Eurogentec) was performed. Blots were developed with the Avidix chemiluminescence detection system (Tropix; Applied Biosystems). To detect the presence of S100A1 on the SDS-PAGE-separated protein mixtures of siRNA experiments, standard Western blotting using an epitope affinity-purified anti-S100A1 antibody (SP5355P, diluted 1:5,000; Acris) was performed (19). Proteins were visualized with a LI-COR infrared imager (Odyssey), and quantitative densitometric analysis was performed by applying Odyssey version 1.2 infrared imaging software. Signals were normalized to calsequestrin densitometric levels that were not different between groups.

Statistical analyses. Data are presented as means ± standard errors of the means (SEM). An unpaired Student *t* test and a two-way repeated analysis of variance were performed to test for differences between groups. A *P* value of <0.01 was accepted as statistically significant.

RESULTS

S100A1 enhances ATP production in neonatal rat cardiomyocytes. To examine the effects of an increased S100A1 protein level on ATP production in NVCMs, cells were transduced by means of an adenoviral construct that independently
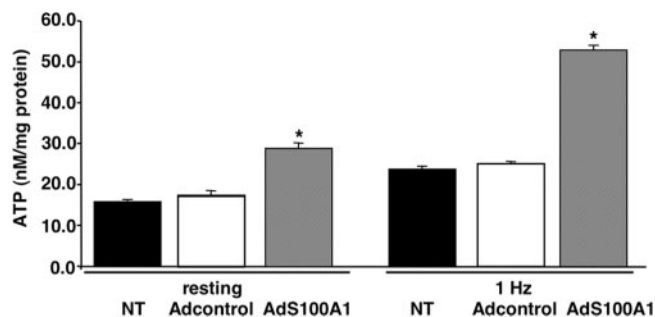

FIG. 1. S100A1 raises the ATP content in neonatal cardiomyocytes. In resting cardiomyocytes, adenovirus-mediated S100A1 overexpression (AdS100A1) led to a significantly higher ATP content (nM/mg protein) than in control transfectants (Adcontrol) and NT cells. Upon electrical stimulation (1 Hz), AdS100A1 cells were able to increase ATP levels to a greater extent than Adcontrol and NT cells. Data are given as means ± SEM for five different experiments.

drives the expression of human S100A1 and GFP (AdS100A1). As a control, NVCMs were infected with the corresponding adenovirus carrying only GFP cDNA (Adcontrol). At 24 hours postinfection, AdS100A1, Adcontrol, and nontransfected (NT) cells were processed for ATP quantification by using a luciferase-based luminometry reaction. Under resting conditions (without electrical stimulation), the amount of ATP was raised by ~67% in AdS100A1 cells compared to that in control cells expressing endogenous S100A1 only (Fig. 1). In response to electrical stimulation at 1 Hz, ATP production was increased by ~110% in cells overexpressing S100A1. These data suggest that S100A1 is involved in the regulation of energy metabolism in NVCMs.

Calcium-dependent interaction of S100A1 with mitochondrial proteins. To identify possible target proteins of S100A1 implicated in the ATP increase observed in S100A1-overexpressing cells, we performed GST-S100A1 pull-down assays with different heart homogenates in the presence of 2 mM $CaCl_2$ or 2 mM EGTA (Fig. 2). Silver-stained protein bands that were specific to GST-S100A1 pull-down assays in the presence of 2 mM $CaCl_2$ were analyzed by mass spectrometry. In homogenates of isolated NVCMs (Fig. 2A), five different mitochondrial proteins, hydroxyl-coenzyme A dehydrogenase, the α-chain of F_1-ATPase, isocitrate dehydrogenase 2, annexin V, and adenine nucleotide translocase, were identified as potential binding partners of S100A1. The corresponding proteins were also pulled down from adult rat heart homogenates (data not shown).

To substantiate the finding that S100A1 interacts with a number of mitochondrial proteins, we isolated mitochondria from adult rat hearts and prepared corresponding mitochondrial extracts for pull-down assays with GST-S100A1 (Fig. 2B). Analyses by mass spectrometry revealed that the S100A1-interacting proteins identified in isolated mitochondria were the same as those detected in isolated NVCMs. In addition, the β-chain of F_1-ATPase (2a) was identified in mitochondrial extracts.

S100A1 colocalizes with F_1-ATPase in mitochondria. We used immunofluorescence and immunoelectron microscopy to probe the cellular distribution of S100A1 and its association with F_1-ATPase in situ. Indirect immunofluorescence
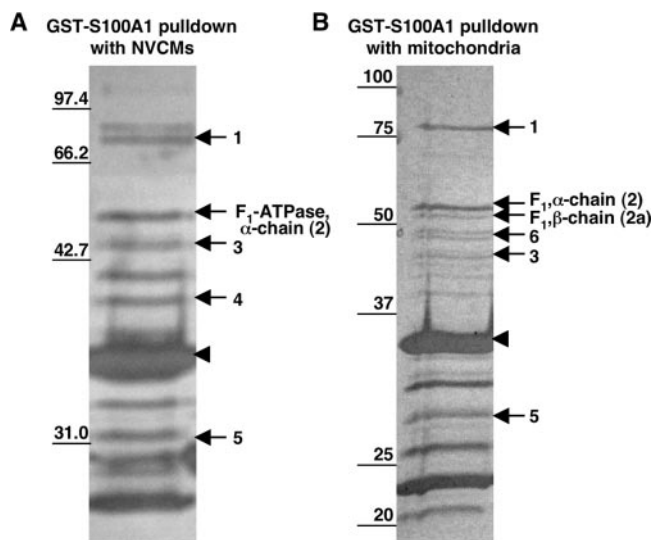
FIG. 2. Results of GST-S100A1 pull-down assays with different homogenates. Protein eluates from different GST-S100A1 pull-down assays were separated on denaturing SDS-polyacrylamide gels and individual proteins identified by mass spectrometry. (A) Five mitochondrial proteins from a homogenate of NVCMs that interact with GST-S100A1 were identified: hydroxyl-coenzyme A dehydrogenase (1), the α-chain of F_1-ATPase (2), isocitrate dehydrogenase 2 (3), annexin V (4), and adenine nucleotide translocase (5). (B) Similar proteins were pulled down from isolated mitochondria by GST-S100A1 in the presence of 2 mM $CaCl_2$. In addition, the β-chain of F_1-ATPase (2a) and the hydroxyacyl dehydrogenase (6) were identified. The band representing GST-S100A1 is indicated by an arrowhead.

labeling of NVCMs with an S100A1 antibody revealed a punctate distribution of S100A1 (green) throughout the cytoplasm (Fig. 3A and D) and, to a lesser extent, in the nucleus. Because NVCMs were incubated in parallel with

MitoTracker Red, mitochondria (red) could be identified as "bullet-shaped" structures (Fig. 3B). Merging the two confocal images revealed a partial colocalization of S100A1 with mitochondria (yellow) (Fig. 3C).

To analyze the interaction of S100A1 and F_1-ATPase at the subcellular level, we performed double immunolabeling experiments with NVCMs with a monoclonal antibody against S100A1 and a polyclonal antibody that reacts with all five subunits of F_1-ATPase. As illustrated in Fig. 3E, the F_1-ATPase antibody typically revealed bullet-shaped structures (blue), which were similar to the mitochondria stained by MitoTracker. Merging the respective confocal images (Fig. 3D and E) clearly showed that S100A1 partially localized to the same confocal volume as F_1-ATPase (turquoise) (Fig. 3F).

To obtain more-detailed information on this colocalization, we used double immunogold labeling of S100A1 and F_1-ATPase on ultrathin sections of a 3-day-old neonatal rat heart. As indicated by the red circles in the electron micrograph displayed in Fig. 3G, we observed numerous cases in which 10-nm gold particles (S100A1) and 5-nm gold particles (F_1-ATPase) appeared in close proximity. With the dimensions of the two antibody complexes being taken into account, a spacing of approximately 30 nm between 10-nm and 5-nm gold particles is indicative of a physical interaction between the two binding sites. In conclusion, these immunolocalization studies substantiated the localization of S100A1 in mitochondria and its direct interaction with F_1-ATPase.

The interaction of S100A1 with the α- and β-chain of F_1-ATPase depends on calcium and pH. To confirm the direct interaction of S100A1 with the α- and β-chain of F_1-ATPase, we performed reverse pull-down assays. For this purpose, recombinant GST–α-chain and GST–β-chain fusion proteins or GST alone was coupled to glutathione-Sepharose beads in the presence of 2 mM $CaCl_2$, 0.2 mM $CaCl_2$, or 2 mM EGTA and subsequently incubated with recombinant S100A1 protein.
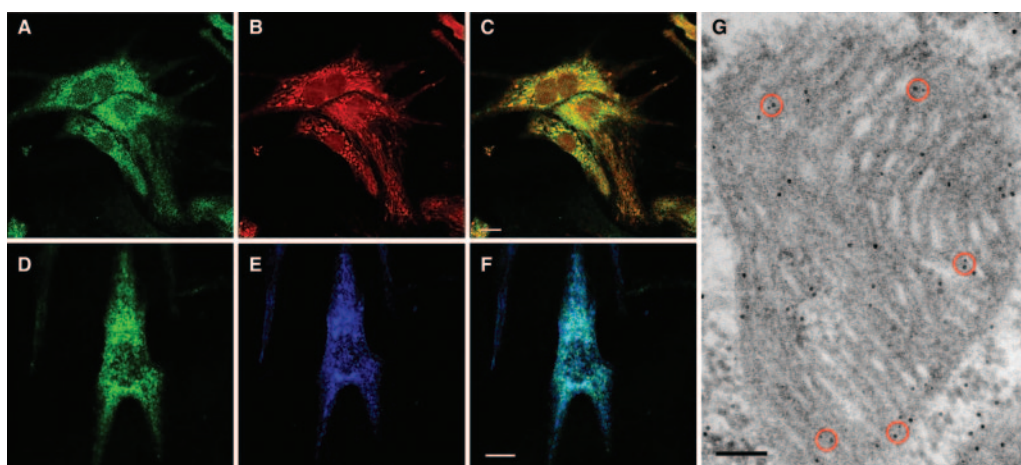

FIG. 3. S100A1 is present in mitochondria, where it colocalizes with F_1-ATPase. (A and D) S100A1 is labeled with a monoclonal S100A1-Alexa 488 mouse antibody in NVCMs (green). (B) Mitochondria were recognized by MitoTracker Red uptake (red). (C) Overlay of panels A and B reveals a partial colocalization of S100A1 with mitochondria (yellow). Bar, 10 μm. (E) F_1-ATPase labeled with a polyclonal F_1-ATPase–Cy5 anti-rabbit antibody (blue). (F) Superposition of panels D and E reveals a partial colocalization of S100A1 and F_1-ATPase (turquoise). Bar, 10 μm. (G) Ultrastructural colocalization of S100A1 and F_1-ATPase in mitochondria from a neonatal rat heart revealed by double immunogold staining. The electron micrograph depicts the colocalization of S100A1 and F_1-ATPase, as indicated by 10-nm and 5-nm gold particles that are less than 30 nm apart (marked as red circles). Bar, 150 nm.
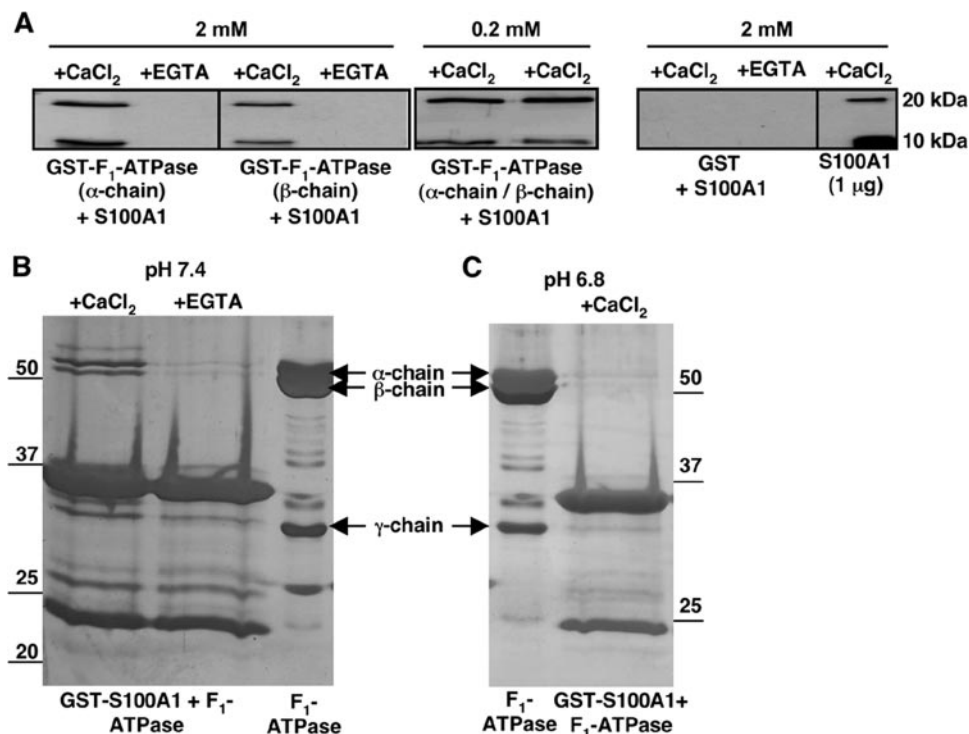
FIG. 4. Results of pull-down assays indicate an interaction between S100A1 and F₁-ATPase. (A) Western blot of eluates of GST–F₁-ATPase α- and β-chain pull-down assays performed with recombinant human S100A1 in the presence of 2 mM CaCl₂, 0.2 mM CaCl₂, or 2 mM EGTA. Probing with an anti-human S100A1-specific antibody revealed 10-kDa (monomeric) and 20-kDa (dimeric) S100A1 species, which were pulled down by the GST–F₁-ATPase α- and β-chain in the presence of 2 mM CaCl₂ and 0.2 mM CaCl₂. GST alone (control) did not pull down S100A1. (B and C) Results of pull-down assays with GST-S100A1 and purified F₁-ATPase at different pHs. (B) At pH 7.4, in the presence of 2 mM CaCl₂, two bands migrating at approximately 55 and 51 kDa were detected. A comparison with purified F₁-ATPase (right lane) indicates that these bands represent the α- and β-chain subunits. EGTA (2 mM) largely abolished the interaction between GST-S100A1 and the α- and β-chain of F₁-ATPase. (C) At pH 6.8, F₁-ATPase subunits were not pulled down by GST-S100A1 even in the presence of 2 mM CaCl₂.

Bound protein was eluted and analyzed by SDS-PAGE and Western blotting using an S100A1 antibody (Fig. 4A).

In the presence of 2 mM CaCl₂ and 0.2 mM CaCl₂, the GST–α-chain and the GST–β-chain fusion protein pulled down two bands with apparent molecular masses of 10 and 20 kDa, respectively, which were recognized by the S100A1 antibody. The migration behavior of these two bands corresponds to that of the monomeric and dimeric forms of recombinant S100A1. Both bands were absent when pull-down assays were carried out in the presence of EGTA or GST control beads.

Furthermore, when GST-S100A1 pull-down assays with purified bovine heart F₁-ATPase were performed under different pH conditions, a pH-sensitive interaction was observed (Fig. 4B and C). At pH 7.4, the α- and β-chain of F₁-ATPase were pulled down by GST-S100A1 in the presence of 2 mM CaCl₂. However, in the presence of 2 mM EGTA, the two respective bands were significantly diminished. When the pH was lowered to 6.8, the binding of F₁-ATPase to GST-S100A1 was barely detectable even in the presence of 2 mM CaCl₂. In control pull-down assays carried out in the presence of 2 mM EGTA or immobilized GST alone, no bands were visible (data not shown). These data confirmed that at pH 7.4, there is a direct interaction between S100A1 and the α- and β-chain of F₁-ATPase in the presence of 2 mM or 0.2 mM CaCl₂.

S100A1 forms a complex with F₁-ATPase and increases its activity. To analyze the interaction of S100A1 and F₁-ATPase

in molecular detail, we isolated the S100A1–F₁-ATPase complex by gel filtration chromatography. For complex formation, purified F₁-ATPase was incubated at pH 7.4 with a 12.5-fold molar excess of S100A1 in the presence of 2 mM CaCl₂ or 2 mM EGTA for 30 min at 37°C. To maintain F₁-ATPase activity, 1 mM MgATP was added to the mixture at 1 and 15 min. After incubation, the mixture was subjected to gel filtration chromatography on a Superdex 200 HiLoad column and individual fractions were analyzed by SDS-PAGE. In the presence of CaCl₂, two prominent peaks were identified in the elution profile (Fig. 5A). Based on the apparent molecular masses of the proteins that eluted in the first peak (fractions 36 to 42), this peak contained the five subunits of F₁-ATPase (α-, β-, γ-, δ-, and ε-chain) and, as suggested by their electrophoretic mobility, monomeric and dimeric S100A1 (10- and 20-kDa bands, respectively) (Fig. 5A). The presence of S100A1 was confirmed by Western blotting using an S100A1-specific antibody and by mass spectrometry (data not shown). The elution profile of peak I also displayed a small shoulder (fractions 40 to 42) that possibly represents aggregation products of S100A1 and F₁-ATPase subunits. SDS-PAGE of the second, smaller peak (fractions 50 to 54) contained predominantly free S100A1 monomers and dimmers and only traces of F₁-ATPase subunits.

In the presence of 2 mM EGTA, gel filtration chromatography of the S100A1–F₁-ATPase complex (Fig. 5B) produced
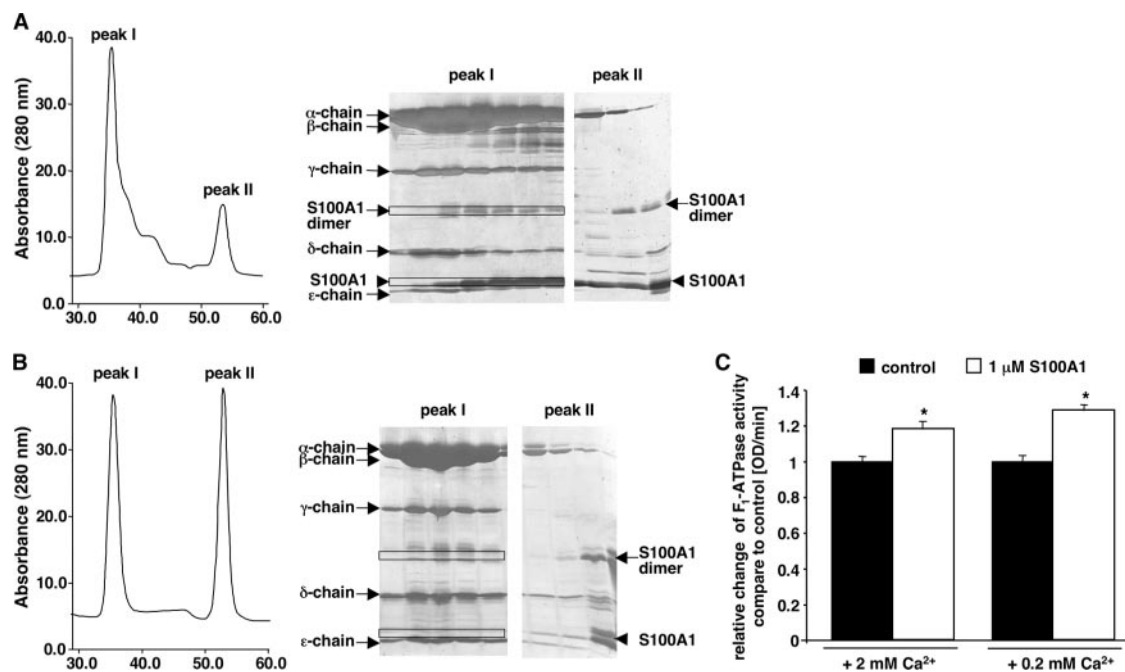
FIG. 5. Results of gel filtration chromatography of the S100A1–F_1-ATPase complex and determination of F_1-ATPase activity. (A) Analysis of the S100A1–F_1-ATPase complex in the presence of 2 mM $CaCl_2$. The absorbance of the eluant was monitored at 280 nm. The elution profile shows two major peaks of different heights. Analysis of individual column fractions (x axis) on a 12 to 22% gradient SDS-PAGE gel reveals that peak I (fractions 36 to 42) contains the five subunits of F_1-ATPase as well as S100A1 in the form of a dimer and a monomer (framed in black). Peak II (fractions 50 to 54) comprises the excess of recombinant S100A1. Only residual amounts of F_1-ATPase subunits were detected in this peak. (B) In the presence of 2 mM EGTA, the elution profile of the S100A1–F_1-ATPase complex displayed two symmetric peaks of comparable heights. The five subunits of F_1-ATPase were eluted in peak I (column fractions 36 to 40), whereas S100A1 protein appeared only in peak II in the form of a monomer and a dimer (fractions 49 to 53). The S100A1 monomer is indicated by an arrowhead. (C) S100A1 increases F_1-ATPase activity. F_1-ATPase activity was measured with an ATP-regenerating system by following the oxidation of NADH to NAD^+ at 340 nm in the presence of either 2 mM or 0.2 mM calcium. Results are reported as relative changes of F_1-ATPase activity in the presence of 1 μM S100A1 compared to F_1-ATPase activity in the control (F_1-ATPase alone). Data are represented as means ± SEM for 25 experiments. *, $P < 0.01$. OD, optical density.

an elution profile that was clearly distinct from that obtained with 2 mM $CaCl_2$. SDS-PAGE analysis of the first peak (fractions 36 to 40) revealed the five subunits of F_1-ATPase but no monomeric or dimeric S100A1 protein. S100A1 eluted only in fractions corresponding to the second peak (fractions 49 to 53). This peak, which contains predominantly the free S100A1, was increased by approximately 150% compared to the corresponding peak obtained in the presence of 2 mM $CaCl_2$ (Fig. 5A, peak II). Together, the data indicate that S100A1 forms a complex with F_1-ATPase in the presence of calcium at pH 7.4.

To determine the functional effects resulting from the interaction of S100A1 with F_1-ATPase, we measured the activity of isolated F_1-ATPase incubated with S100A1 (Fig. 5C). Accordingly, S100A1 caused an ~18% increase in F_1-ATPase activity in the presence of 2 mM $CaCl_2$ and an ~28% increase in the presence of 0.2 mM $CaCl_2$.

In conclusion, these studies substantiate the direct interaction of S100A1 with F_1-ATPase and its effects on F_1-ATPase activity.

S100A1 protein levels affect ATP synthase activity, ATP content, and Ca^{2+} transient amplitudes in cardiomyocytes. To address the functional significance of an S100A1–F_1-ATPase interaction in cells, we examined the consequences of S100A1 knockdown on both ATP synthase activity and F_1-ATPase-mediated ATP production in cardiomyocytes.

To examine the relationship between S100A1 levels and ATP

synthase activity, we used adult ventricular cardiomyocytes from WT and SKO (5) mice. The significantly higher conversion rate of NADH to NAD^+ observed in WT than in SKO cardiomyocyte homogenates at 0.2 μM and 0.2 mM free $[Ca^{2+}]$ indicated a higher mitochondrial ATP synthase activity in WT cardiomyocytes (Fig. 6A). Because cardiomyocyte homogenates were prepared in Ca^{2+}-buffered solution, which prevented the loss of endogenous S100A1 protein in WT cardiomyocytes as confirmed by immunoblotting (data not shown), the higher ATP synthase activity could be attributed to S100A1. Consistently, the addition of recombinant S100A1 protein to SKO cardiomyocyte homogenates significantly increased mitochondrial ATP synthase activity at both 0.2 μM and 0.2 mM free $[Ca^{2+}]$.

To analyze the ATP content in cardiomyocytes expressing different S100A1 protein levels, NVCMs were transfected with S100A1 siRNA or scrambled control RNA. The efficient suppression of S100A1 protein by the specific siRNA in transfected NVCMs was confirmed by Western blotting (Fig. 6B). Parallel NVCM cultures were lysed at 72 hours posttransfection, and subsequently, ATP levels were assayed by a luciferase-based luminometry reaction. As illustrated in Fig. 6B, knockdown of S100A1 expression in unstimulated NVCMs (S100A1 siRNA, basal conditions) caused ATP levels to decrease by an average of 48% compared to those in control cells transfected with scrambled siRNA or those in NT NVCMs. Consistent with the notion that S100A1 levels influence ATP production, overexpression of
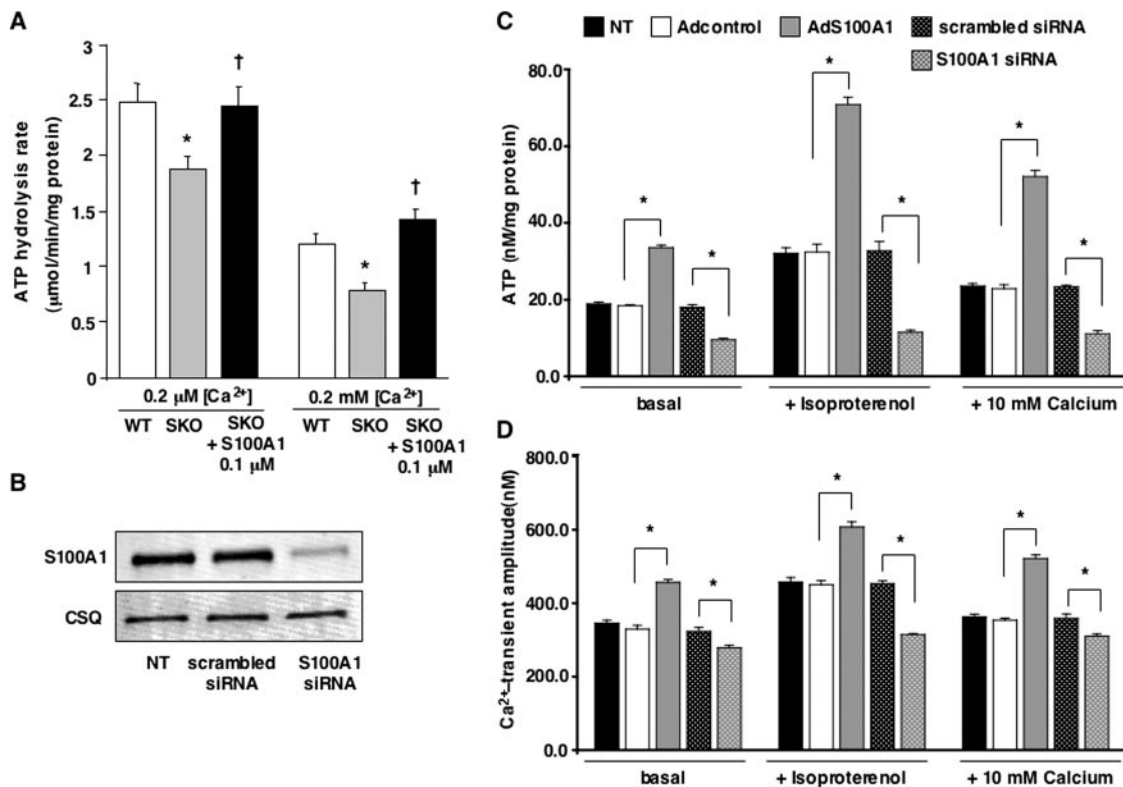
FIG. 6. S100A1 protein levels affect ATP synthase activity, ATP content, and Ca^{2+} transient amplitudes of cardiomyocytes. (A) Mitochondrial ATP synthase activity assessed by monitoring the conversion of NADH to NAD$^+$ in WT and SKO cardiomyocyte homogenates. Mitochondrial ATP synthase activity is significantly lower in SKO cardiomyocyte homogenates at 0.2 μM and 0.2 mM free [Ca^{2+}] than in the WT. Preincubation with S100A1 protein (0.1 μM) for 10 min restored mitochondrial ATP synthase activity in SKO cardiomyocyte homogenates at 0.2 μM and 0.2 mM free [Ca^{2+}]. Values are means ± SEM. ∗, $P < 0.05$ versus WT cardiomyocytes; †, $P < 0.05$ versus SKO cardiomyocytes. Each experiment was carried out in triplicate ($n = 4$ cell preparations). (B) Western blot of S100A1 or calsequestrin (CSQ) (loading control) of extracts from cells transfected with scrambled or S100A1 siRNA or NT cells. (C) Comparison of the ATP content in NT, adenovirus-transduced (AdS100A1 and Adcontrol), and siRNA-treated cells. Under basal conditions, S100A1 overexpression (AdS100A1) resulted in a significantly higher ATP content than in control (Adcontrol) and NT cells. In contrast, knockdown of S100A1 protein (S100A1 siRNA) led to a significant reduction of ATP compared to that in control cells (scrambled siRNA). Upon isoproterenol stimulation, AdS100A1 cells exhibited a twofold-higher ATP content than Adcontrol and NT cells, whereas S100A1 suppression caused a twofold reduction of ATP compared to what was observed for scrambled siRNA-treated cells. The addition of 10 mM calcium also yielded a twofold increase of ATP content in AdS100A1 cells and likewise a twofold reduction in S100A1 siRNA cells. (D) Effects of S100A1 protein levels on Ca^{2+} transients. Compared to control cells expressing endogenous levels of S100A1, S100A1 overexpression (AdS100A1) significantly increased the Ca^{2+} transient amplitude under basal conditions as well as when stimulated with isoproterenol or 10 mM calcium. Suppression of S100A1 protein led to decreased Ca^{2+} transient amplitude. Data are represented as means ± SEM for five different experiments in panel C and for 150 cells from the different cell preparations in panel D. ∗, $P < 0.01$.

S100A1 in NVCMs (AdS100A1) (Fig. 6C) increased ATP levels by 82% compared to those in control cells expressing endogenous S100A1 (Adcontrol and NT) (Fig. 6C). Qualitatively similar results were obtained after the stimulation of cells with 1 μM isoproterenol, a beta-adrenergic receptor agonist, or 10 mM CaCl$_2$: S100A1-deficient NVCMs exhibited significantly reduced ATP levels (approximately 65% for isoproterenol-treated and 53% for CaCl$_2$-treated knockdown NVCMs compared to the level for control cells), whereas overexpression of S100A1 consistently led to enhanced ATP levels (approximately 118% for isoproterenol-treated and 127% for CaCl$_2$-treated AdS100A1 NVCMs compared to the level for control cells). Furthermore, compared to control or AdS100A1 cells, S100A1-deficient NVCMs were not able to respond with an adequate ATP increase after isoproterenol or CaCl$_2$ stimulation.

To examine the effects of reduced and increased levels of S100A1 on Ca^{2+} cycling, we recorded Ca^{2+} transients in NVCMs under basal and stimulated conditions (Fig. 6D). In AdS100A1 cells overexpressing S100A1, the increased ATP content was accompanied by an increase in Ca^{2+} transient amplitudes compared to what was observed for control cells (approximately 38% increase for basal, 35% for isoproterenol-treated, and 47% for CaCl$_2$-treated AdS100A1 cells). Consistently, the suppression of S100A1 protein by S100A1 siRNA led to decreased Ca^{2+} transient amplitudes (approximately 14% for basal, 30% for isoproterenol-treated, and 12% for CaCl$_2$-treated AdS100A1 cells compared to the amplitude for control cells), concomitant with reduced ATP production.

DISCUSSION

S100A1 has recently been recognized to act as a regulator of Ca^{2+} cycling and contractility in the heart (15, 20, 23). However, efficient performance of the myocardium, in particular

cardiac contractility, is based not only on Ca^{2+} homeostasis but to a large extent also on energy metabolism (reviewed in references 6 and 10). Thus, the increase in cardiac contractility brought on by S100A1 overexpression strongly argued for a role for S100A1 in energy metabolism in addition to its role in Ca^{2+} cycling. Indeed, we found that the ATP content measured in cardiomyocytes overexpressing S100A1 (AdS100A1) was 67% higher in resting AdS100A1 cells and even 110% higher in electrically stimulated AdS100A1 cells than in control cells. This ATP increase substantiates the notion that S100A1 is involved in the regulation of energy metabolism in cardiomyocytes.

Pull-down experiments with GST-S100A1 provided the first clues as to the molecular mechanism underlying the increase in ATP induced by S100A1. Interestingly, several mitochondrial proteins were pulled down by GST-S100A1, and virtually all of these potential S100A1 target proteins are involved in the cell's energy metabolism. In support of our findings, gel overlay experiments revealed glycogen phosphorylase and phosphoglucomutase, which, through their role in glycogenolysis, are also involved in energy production as potential target proteins of S100A1 (31). In addition, S100A1 was shown to interact in a Ca^{2+}-dependent manner with fructose-1,6-bisphosphate aldolase, thereby increasing its enzymatic activity (32). Fructose-1,6-bisphosphate aldolase is a key regulator of glycolysis and is thus essential for energy production. Our data provide the first evidence that S100A1 interacts in a Ca^{2+}-dependent manner with F_1-ATPase in heart tissue. F_1-ATPase is part of the F_1F_o-ATPase, which is responsible for ATP synthesis in the cell. Hence, it is tempting to speculate that the interaction of S100A1 with F_1-ATPase is responsible for the increased ATP content in cardiomyocytes overexpressing S100A1. At this point, we cannot rule out that any of the other mitochondrial proteins pulled down by GST-S100A1, for example, the Ca^{2+}-sensitive dehydrogenase isocitrate and the adenine nucleotide translocase, could also play a role in regulating the ATP content of the cell.

Because we were able to demonstrate a direct interaction of S100A1 with the α- and β-chain of F_1-ATPase by reverse pull-down assays using the GST–F_1-ATPase α- and β-chain as bait proteins for recombinant S100A1, we have focused our studies on the S100A1–F_1-ATPase interaction. The specificity of this interaction was corroborated by the Ca^{2+} dependence and pH sensitivity of S100A1 binding to the α- and β-chain of F_1-ATPase. The most convincing piece of evidence that S100A1 biochemically interacts with F_1-ATPase has been provided by the isolation of an S100A1–F_1-ATPase complex by gel filtration chromatography.

For a physical interaction of S100A1 and F_1-ATPase to occur in the cell, the spatial proximity of these proteins is required. While the localization of F_1-ATPase in mitochondria has been known for quite some years (13), there are only a limited number of studies that report a mitochondrial localization of S100A1. For example, electron microscopy studies have shown that S100A1 is present in the mitochondria of mouse slow-twitch fibers (8) as well as in mitochondria of the human heart (14). Similarly, our data document the presence of S100A1 at the inner and outer mitochondrial membranes as well as in the matrix of rat heart mitochondria. Furthermore, double immunolabeling experiments from both confocal light and electron microscopy studies reveal that S100A1 and F_1-ATPase indeed colocalize in mitochondria, indicating that a physical interaction between S100A1 and F_1-ATPase is likely to occur in vivo.

A first indication of the functional significance of such an interaction has been reported by Simonian et al., who showed that S100A1 stimulated the ATPase activity in mitochondria isolated from gerbil brain (26). The increased level of ATP we observed in cardiomyocytes that overexpress S100A1 extends the notion of a functional interaction between S100A1 and F_1-ATPase. Moreover, the effect of S100A1 knockdown on the ATP level consolidates the association of S100A1 with mitochondrial ATP production. Further evidence is provided by the diminished mitochondrial ATPase activity observed in cardiomyocytes from S100A1 knockout mice. A direct indication of the influence of S100A1 on the function of F_1-ATPase is provided by the determination of F_1-ATPase activity. Indeed, the incubation of S100A1 with isolated F_1-ATPase causes an 18% increase in F_1-ATPase activity in the presence of 2 mM $CaCl_2$ and a 28% increase at 0.2 mM calcium. The direct impact of S100A1 protein on F_1-ATPase activity is also demonstrated by restoring decreased mitochondrial ATP synthase activity in SKO cardiomyocytes through exogenous S100A1.

A potential interaction between the Ca^{2+}-binding protein S100A1 and F_1-ATPase raises the question of how energy production, as well as cardiac work, and Ca^{2+} homeostasis are connected. In their recent work, Ventura-Clapier et al. have suggested that Ca^{2+} is one of the main candidates for coupling energy metabolism and cardiac work (reviewed in reference 29). Furthermore, work by Territo et al. and Balaban has shown that cytosolic Ca^{2+} plays an important role in the regulation of cardiac energy metabolism. Of particular interest is their finding that Ca^{2+} activates several steps in oxidative phosphorylation, including F_1F_o-ATPase (27, 28; reviewed in reference 1). It has been proposed that Ca^{2+} as an intermediary may concomitantly control both energy metabolism and cardiac work (28). Because S100A1 not only improves cardiac Ca^{2+} handling and heart muscle contractility (19) but also increases energy production, we speculate that the Ca^{2+} sensor might be involved in coupling Ca^{2+} cycling with Ca^{2+}-dependent regulation of cardiac metabolism. This notion is supported by the finding that Ca^{2+} transient amplitudes and ATP levels were concomitantly increased when S100A1 levels were raised, whereas knockdown of S100A1 reduced both ATP levels and Ca^{2+} transient amplitudes. The important question of whether improved energy supply is crucial to S100A1 Ca^{2+}-dependent inotropic actions in healthy and diseased myocardia will need to be addressed in future studies.

In conclusion, our data have unveiled a novel role for S100A1 in cardiac metabolism. Undoubtedly, more-detailed knowledge of the molecular interaction between F_1-ATPase and S100A1 and also the other mitochondrial target proteins identified by pull-down assays is needed to more rationally understand the molecular mechanism by which S100A1 participates in cardiac energy metabolism. Elucidation of this molecular mechanism will ultimately provide insight into the failing heart where the cardiac pump is no longer able to meet the energy requirements of the body.

REFERENCES

1. **Balaban, R. S.** 2002. Cardiac energy metabolism homeostasis: role of cytosolic calcium. J. Mol. Cell. Cardiol. **34:**1259–1271.
2. **Bosetti, F., G. Yu, R. Zucchi, S. Ronca-Testoni, and G. Solaini.** 2000. Myocardial ischemic preconditioning and mitochondrial F1F0-ATPase activity. Mol. Cell. Biochem. **215:**31–37.
3. **Cadenas, S., and M. D. Brand.** 2000. Effects of magnesium and nucleotides on the proton conductance of rat skeletal-muscle mitochondria. Biochem. J. **348:**209–213.
4. **Donato, R.** 2003. Intracellular and extracellular roles of S100 proteins. Microsc. Res. Tech. **60:**540–551.
5. **Du, X. J., T. J. Cole, N. Tenis, X. M. Gao, F. Kontgen, B. E. Kemp, and J. Heierhorst.** 2002. Impaired cardiac contractility response to hemodynamic stress in S100A1-deficient mice. Mol. Cell. Biol. **22:**2821–2829.
6. **Duchen, M. R.** 2004. Roles of mitochondria in health and disease. Diabetes **53**(Suppl. 1):S96–S102.
7. **Florholmen, G., V. Aas, A. C. Rustan, P. K. Lunde, N. Straumann, H. Eid, A. Odegaard, H. Dishington, K. B. Andersson, and G. Christensen.** 2004. Leukemia inhibitory factor reduces contractile function and induces alterations in energy metabolism in isolated cardiomyocytes. J. Mol. Cell. Cardiol. **37:**1183–1193.
8. **Haimoto, H., and K. Kato.** 1987. S100a0 (alpha alpha) protein, a calcium-binding protein, is localized in the slow-twitch muscle fiber. J. Neurochem. **48:**917–923.
9. **Heizmann, C. W., and J. A. Cox.** 1998. New perspectives on S100 proteins: a multi-functional Ca(2+)-, Zn(2+)- and Cu(2+)-binding protein family. Biometals **11:**383–397.
10. **Huss, J. M., and D. P. Kelly.** 2005. Mitochondrial energy metabolism in heart failure: a question of balance. J. Clin. Investig. **115:**547–555.
11. **Ingwall, J. S., and R. G. Weiss.** 2004. Is the failing heart energy starved? On using chemical energy to support cardiac function. Circ. Res. **95:**135–145.
12. **Kato, K., and S. Kimura.** 1985. S100ao (alpha alpha) protein is mainly located in the heart and striated muscles. Biochim. Biophys. Acta **842:**146–150.
13. **Lehninger, A. L.** 1967. Energy coupling in electron transport. Fed. Proc. **26:**1333–1334.
14. **Maco, B., A. Mandinova, M. B. Durrenberger, B. W. Schafer, B. Uhrik, and C. W. Heizmann.** 2001. Ultrastructural distribution of the S100A1 Ca2+-binding protein in the human heart. Physiol. Res. **50:**567–574.
15. **Most, P., J. Bernotat, P. Ehlermann, S. T. Pleger, M. Reppel, M. Borries, F. Niroomand, B. Pieske, P. M. Janssen, T. Eschenhagen, P. Karczewski, G. L. Smith, W. J. Koch, H. A. Katus, and A. Remppis.** 2001. S100A1: a regulator of myocardial contractility. Proc. Natl. Acad. Sci. USA **98:**13889–13894.
16. **Most, P., M. Boerries, C. Eicher, C. Schweda, P. Ehlermann, S. T. Pleger, E. Loeffler, W. J. Koch, H. A. Katus, C. A. Schoenenberger, and A. Remppis.** 2003. Extracellular S100A1 protein inhibits apoptosis in ventricular cardiomyocytes via activation of the extracellular signal-regulated protein kinase 1/2 (ERK1/2). J. Biol. Chem. **278:**48404–48412.
17. **Most, P., M. Boerries, C. Eicher, C. Schweda, M. Volkers, T. Wedel, S. Sollner, H. A. Katus, A. Remppis, U. Aebi, W. J. Koch, and C. A. Schoenenberger.** 2005. Distinct subcellular location of the Ca2+-binding protein S100A1 differentially modulates Ca2+-cycling in ventricular rat cardiomyocytes. J. Cell Sci. **118:**421–431.
18. **Most, P., and W. J. Koch.** 2007. S100A1: a calcium-modulating inotropic prototype for future clinical heart failure therapy. Future Cardiol. **3:**5–11.
19. **Most, P., S. T. Pleger, M. Volkers, B. Heidt, M. Boerries, D. Weichenhan, E. Loffler, P. M. Janssen, A. D. Eckhart, J. Martini, M. L. Williams, H. A. Katus, A. Remppis, and W. J. Koch.** 2004. Cardiac adenoviral S100A1 gene delivery rescues failing myocardium. J. Clin. Investig. **114:**1550–1563.
20. **Most, P., A. Remppis, S. T. Pleger, E. Loffler, P. Ehlermann, J. Bernotat, C. Kleuss, J. Heierhorst, P. Ruiz, H. Witt, P. Karczewski, L. Mao, H. A. Rockman, S. J. Duncan, H. A. Katus, and W. J. Koch.** 2003. Transgenic overexpression of the Ca2+-binding protein S100A1 in the heart leads to increased in vivo myocardial contractile performance. J. Biol. Chem. **278:**33809–33817.
21. **Most, P., H. Seifert, E. Gao, H. Funakoshi, M. Volkers, J. Heierhorst, A. Remppis, S. T. Pleger, B. R. DeGeorge, Jr., A. D. Eckhart, A. M. Feldman, and W. J. Koch.** 2006. Cardiac S100A1 protein levels determine contractile performance and propensity toward heart failure after myocardial infarction. Circulation **114:**1258–1268.
22. **Orriss, G. L., A. G. Leslie, K. Braig, and J. E. Walker.** 1998. Bovine F1-ATPase covalently inhibited with 4-chloro-7-nitrobenzofurazan: the structure provides further support for a rotary catalytic mechanism. Structure **6:**831–837.
23. **Remppis, A., P. Most, E. Loffler, P. Ehlermann, J. Bernotat, S. Pleger, M. Borries, M. Reppel, J. Fischer, W. J. Koch, G. Smith, and H. A. Katus.** 2002. The small EF-hand Ca2+ binding protein S100A1 increases contractility and Ca2+ cycling in rat cardiac myocytes. Basic Res. Cardiol. **97**(Suppl. 1)**:**I56–I62.
24. **Sambrano, G. R., I. Fraser, H. Han, Y. Ni, T. O'Connell, Z. Yan, and J. T. Stull.** 2002. Navigating the signalling network in mouse cardiac myocytes. Nature **420:**712–714.
25. **Schoenenberger, C. A., S. Buchmeier, M. Boerries, R. Sutterlin, U. Aebi, and B. M. Jockusch.** 2005. Conformation-specific antibodies reveal distinct actin structures in the nucleus and the cytoplasm. J. Struct. Biol. **152:**157–168.
26. **Simonian, A., J. Baudier, and K. G. Haglid.** 1989. Modulation of ATPase activities in the central nervous system by the S-100 proteins. Neurochem. Res. **14:**761–764.
27. **Territo, P. R., S. A. French, M. C. Dunleavy, F. J. Evans, and R. S. Balaban.** 2001. Calcium activation of heart mitochondrial oxidative phosphorylation: rapid kinetics of mVO2, NADH, and light scattering. J. Biol. Chem. **276:**2586–2599.
28. **Territo, P. R., V. K. Mootha, S. A. French, and R. S. Balaban.** 2000. Ca(2+) activation of heart mitochondrial oxidative phosphorylation: role of the F(0)/F(1)-ATPase. Am. J. Physiol. Cell Physiol. **278:**C423–C435.
29. **Ventura-Clapier, R., A. Garnier, and V. Veksler.** 2004. Energy metabolism in heart failure. J. Physiol. **555:**1–13.
30. **Zimmer, D. B., E. H. Cornwall, A. Landar, and W. Song.** 1995. The S100 protein family: history, function, and expression. Brain Res. Bull. **37:**417–429.
31. **Zimmer, D. B., and J. G. Dubuisson.** 1993. Identification of an S100 target protein: glycogen phosphorylase. Cell Calcium **14:**323–332.
32. **Zimmer, D. B., and L. J. Van Eldik.** 1986. Identification of a molecular target for the calcium-modulated protein S100. Fructose-1,6-bisphosphate aldolase. J. Biol. Chem. **261:**11424–11428.